Synthesis And Surface Modification of Cellulose Aerogel from Coconut Peat for Oil Adsorption

Phat Nam La
Ho Chi Minh City University of Technology: Truong Dai hoc Bach khoa Dai hoc Quoc gia Thanh pho Ho Chi Minh

Nguyen Cam Huynh
Ho Chi Minh City University of Technology: Truong Dai hoc Bach khoa Dai hoc Quoc gia Thanh pho Ho Chi Minh

Khoa Dang Dang Bui
Ho Chi Minh City University of Technology: Truong Dai hoc Bach khoa Dai hoc Quoc gia Thanh pho Ho Chi Minh

Khang Tan Pham
Ho Chi Minh City University of Technology: Truong Dai hoc Bach khoa Dai hoc Quoc gia Thanh pho Ho Chi Minh

Tien Xuan Dao
Ho Chi Minh City University of Natural Sciences: Truong Dai hoc Khoa hoc Tu nhien Dai hoc Quoc gia Thanh pho Ho Chi Minh

Thang Quoc Tran
Ho Chi Minh City University of Natural Sciences: Truong Dai hoc Khoa hoc Tu nhien Dai hoc Quoc gia Thanh pho Ho Chi Minh

Trung Kim Nguyen
Ho Chi Minh City University of Technology: Truong Dai hoc Bach khoa Dai hoc Quoc gia Thanh pho Ho Chi Minh

Nam Minh Hoang
Ho Chi Minh City University of Technology: Truong Dai hoc Bach khoa Dai hoc Quoc gia Thanh pho Ho Chi Minh

Phong Thanh Mai
Ho Chi Minh City University of Technology: Truong Dai hoc Bach khoa Dai hoc Quoc gia Thanh pho Ho Chi Minh

Hieu Huu Nguyen (nhhieubk@hcmut.edu.vn)
Ho Chi Minh City University of Technology: Truong Dai hoc Bach khoa Dai hoc Quoc gia Thanh pho Ho Chi Minh

---

Research Article

Keywords: Coconut peat, biomass, cellulose aerogel, oil adsorption.

Posted Date: June 4th, 2021

DOI: https://doi.org/10.21203/rs.3.rs-445439/v1

Synthesis And Surface Modification of Cellulose Aerogel from Coconut Peat or Oil Adsorption

La Nam Phat[1,2,4], Huynh Cam Nguyen[1,2,4], Bui Dang Dang Khoa[1,2,4], Pham Tan Khang[1,2,4], Dao Xuan Tien[1,3], Tran Quoc Thang[1,3], Nguyen Kim Trung[2,4], Hoang Minh Nam[2,4], Mai Thanh Phong[2,4], and Nguyen Huu Hieu[1,2,4*]

[1]*VNU-HCM, Key Laboratory of Chemical Engineering and Petroleum Processing (CEPP), Ho Chi Minh City University of Technology (HCMUT)*

268 Ly Thuong Kiet Street, District 10, Ho Chi Minh City, Vietnam

[2]*Faculty of Chemical Engineering, Ho Chi Minh City University of Technology (HCMUT)*

268 Ly Thuong Kiet Street, District 10, Ho Chi Minh City, Vietnam

[3]*Faculty of Chemistry Ho Chi Minh City University of Science (HCMUS)*

227 Nguyen Van Cu Street, District 5, Ho Chi Minh City, Vietna

[4]*Vietnam National University Ho Chi Minh City, Linh Trung Ward, Thu Duc District, Ho Chi Minh City, Vietnam*

*Corresponding author: nhhieubk@hcmut.edu.vn

ABSTRACT

Oil spillage is one of the world's biggest environmental problems, its various impacts including shifting the balance of the ecosystem, affecting marine animals, and inhibiting economical activities. Therefore, the efficient resolution of this issue is a topic of great interest. In this work, the solution of choice is an adsorption method using aerogels made from coconut peat. Cellulose coconut peat aerogels (CCPA) are synthesized by cross-linking method with poly(vinyl alcohol) (PVA) and freeze-drying technique to form the porous structure. The CCPA are furthermore dip-coated in poly(dimethylsiloxane) (PDMS) to obtain PDMS-coated cellulose coconut peat aerogel (CCPA-P) with hydrophobic properties for the studying of oil adsorption. The characteristics of CCPA and CCPA-P are evaluated by density and porosity, specific surface area following Brunauer-Emmett-Teller (BET) theory, scanning electron microscopy (SEM), Fourier-transform infrared spectroscopy (FTIR), X-ray diffraction (XRD), energy dispersive X-ray analysis (EDX), and water contact angle (WCA) measurements. Results showed that CCPA-10 with the mass ratios of cellulose to PVA 10:1 had the lowest density of 28.21 mg/cm^3, highest porosity of 98.15 %. Furthermore, the modified CCPA-P10 had maximum adsorption capacity of up to 2.083 and 2.452 mg/mg for the static adsorption model and dynamic adsorption model, respectively. This indicates that coconut peat is a viable material for aerogel synthesis in oil adsorption applications.

Keywords: Coconut peat, biomass, cellulose aerogel, oil adsorption.

1. INTRODUCTION

With the growth of the automotive industry, oil demand has skyrocketed, leading to numerous oil spill incidents. Recent cases include Prestige spilling 77,000 tons of oil off northwestern Spain (2002), the Hebei Spirit spilling 2.7 million gallons of oil into the Southwest Sea of South Korea (2007), and

the Deepwater Horizon oil spill disaster (2010) in the Gulf of Mexico with the leakage of more than 2.6 million liters of oil – all of which have caused an imbalance to the native ecosystems and obstructed marine economic activities (Trevathan and Viestenz 2019). As such, much research and development of effective and cost-efficient approaches to successfully separate oil from water have been taking place worldwide. Adsorption techniques are considered among these solutions - one of the most effective approaches, due to their simple operation, low cost, non-toxicity, and large adsorption capacity (De Gisi et al. 2016). In addition, due to being an environmentally-friendly material and having excellent adsorbent quality, cellulose aerogels have great potential in the adsorption applications.

Cellulose aerogel – a highly porous and low-density solid material fabricated from cellulose can hold up to 99% by volume of air within their pores (Aegerter et al. 2011). These materials have potential to become adsorbents since they exhibit ultra-low density, high porosity, and large surface area. The mechanism of oil adsorption by aerogels is considered to be governed mainly by aerogel surface adsorption, absorption, hydrophobicity, and diffusion through the voids via inter-fiber capillary action (Carmody et al. 2007; Udayana et al. 2017; Rojas-Valencia et al. 2018). The amount adsorbed is known to be dependent on the surface area and porosity of adsorbents (Feng et al. 2016). On the other hand, coconut peat, otherwise known as agricultural waste, is causing agricultural land unproductivity during the wet season due to tannins and phenols from the coconut peat seeping into the soil (Zhang et al. 2019). While recognizing the escalating problem that peat wastes can cause to the environment, their rich cellulose content means coconut peat has potential in the synthesis of green adsorbents for oil spillage treatment. This has implored coconut peat to be chosen as the raw material to synthesize cellulose aerogels for oil adsorption (Yue et al. 2018).

In this study, 3D network cellulose coconut peat aerogels (CCPA) were fabricated through cross-linking method with poly(vinyl alcohol) (PVA) as a cross-linker, followed by a freeze-drying technique. Additionally, to provide water resistance, CCPA were modified via dip-coating in poly(dimethylsiloxane) (PDMS) to obtain PDMS-coated cellulose coconut peat aerogel (CCPA-P). Characteristics of CCPA and CCPA-P were investigated by density and porosity, specific surface area following Brunauer-Emmett-Teller (BET) theory, scanning electron microscopy (SEM), Fourier-transform infrared spectroscopy (FTIR), X-ray diffraction (XRD), energy dispersive X-ray analysis (EDX), and water contact angle (WCA). The oil adsorption test of CCPA-P was performed through static and dynamic models. Finally, to analyze the adsorption mechanism of the CCPA-P, the pseudo-first-order and the pseudo-second-order models were considered. The schematic illustration of the synthesis route and adsorption process of the CCPA-P is shown in Figure 1.

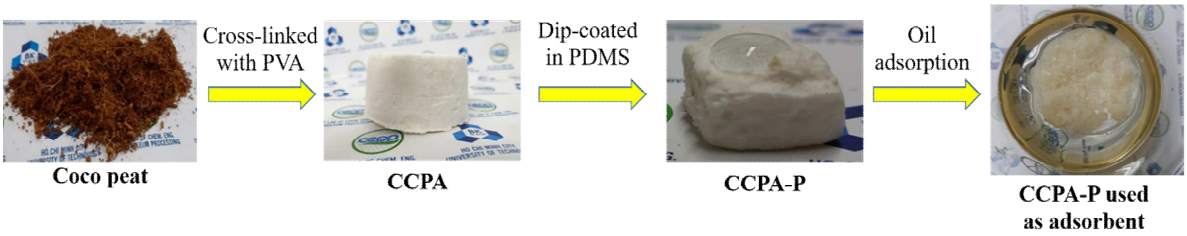

Figure 1. Schematic illustration of the synthesis route and adsorption process of the PPCA-P

2. EXPERIMENTAL

2.1. Materials and chemicals

Sodium hydroxide (NaOH), hydrogen peroxide (H_2O_2), hexane (C_6H_{14}), and PVA were purchased from Xilong Scientific (China). PDMS was bought from Acros Organic, tetraethoxysilane (TEOS) was purchased from Macklin, and dibutyltin dilaurate (DBTL) was bought from Sigma – Aldrich. All solutions were made with deionized water (DI). Used lubricating oils were taken from Saigon Petro.

2.2. Preparation of CCPA

Firstly, coconut peat was soaked in NaOH solution (2 M) with a mass to volume ratio of 1:30 g:mL, then heated at 80 °C for 2 hours. 30 mL of H_2O_2 (30 wt.%) was added, and the mixture was heated at 80 °C for 2 hours and washed with DI water to pH 7 then drying at 60 °C for 24 hours to gain the cellulose material. Subsequently, the obtained cellulose was soaked in PVA solution according to the cellulose to PVA ratios presented in Table 1. The mixture was elevated to 80 °C for 2 hours to promote cross-linking, then sonicated to homogenize the mixture and to remove air bubbles. Freeze-drying the mixture results in the coconut peat cellulose aerogels, labelled consequently CCPA-05, CCPA-10, CCPA-15, CCPA-20, CCPA-25, and CCPA-30.

Table 1. Ratios of cellulose to PVA

Samples	CCPA-05	CCPA-10	CCPA-15	CCPA-20	CCPA-25	CCPA-30
Cellulose:PVA(g:g)	5:1	10:1	15:1	20:1	25:1	30:1
pH			7			

2.3. Preparation of CCPA-P

10 mL of PDMS solution and 25 mL of hexane solvent were stirred together at 30 °C. 3.8 g of TEOS and 0.05 mL of DBTL catalyst were continuously added and stirred at 30 °C for 4 hours. CCPA samples with various cellulose-to-PVA ratios were dipped into the solution and dried at 90 °C for 12 hours. The obtained hydrophobic CCPA samples were named CCPA-P05, CCPA-P10, CCPA-P15, CCPA-P20, CCPA-P25, and CCPA-P30, relative to their CCPA precursors.

2.4. Characterization

SEM (Hitachi S4800, Japan) was employed to observe the morphologies of CCPA. The elemental composition of CCPA was analyzed by EDX mapping (Jeol JSM 6490, Japan). Functional groups of the coconut peat, cellulose, CCPA and CCPA-P were verified by FT-IR spectroscopy (Bruker TENSOR-27, Germany) using potassium bromide (KBr) pellets with various controlling parameters: a

wavenumber region of 400–4000 cm^{-1}, spectrum accuracy of 0.1% T, and resolution of 0.2 cm^{-1}. Diffraction analysis was performed using XRD patterns (Bruker XRD D8, Germany) with operating parameters including CuK_α irradiation (λ_X = 0.154 nm) in the range of 0-80° with a scanning speed of 2°/minute; maximum operating temperature of 30 °C; and maximum humidity of 70%. The water contact angle of CCPA-P was measured (DATAPHYSICS OCA-20, Germany) with a magnification of 0.7–4.5 times. The specific surface area and pore size following BET theory was determined via the nitrogen adsorption/desorption curves at p_0 = 756 mmHg and 77.35 K.

2.5. Density and porosity

The mass and dimension of CCPA were measured using a four-digit balance (CPA225D, Germany) and electronic clamp (VOREL-15240 - 150 mm, Germany), respectively. Densities of CCPA were calculated by Equation (1):

$$\rho = \frac{m}{V} \tag{1}$$

while m (mg) is the weight of the materials and V (cm^3) is the aerogels volume obtained by Equation (2):

$$V = \frac{\pi d^2 h}{4} \tag{2}$$

where d (mm) and h (mm) represent the diameter and height of the aerogels, respectively.

The porosities of CCPA and CCPA-P (θ) were determined according to Equation (3):

$$\theta\ (\%) = 100 \times \left(1 - \frac{\rho}{\rho_s}\right) \tag{3}$$

while ρ is the density of the aerogels and ρ_s is the density of the solid material.

2.6. Oil adsorption test

The oil adsorption capacity of CCPA-P was investigated via a static model. The samples were placed on the surface of the oil-water mixture with time from 1 to 10 minutes. After the adsorption test, the samples were removed and weighed. The oil adsorption capacity was calculated via Equation 4.

$$Q = \frac{W_s - W_t}{W_t} \tag{4}$$

where Q (mg/g) is the oil adsorption capacity of the sample, W_s (mg) and W_t (mg) are the mass of the sample before and after being tested, accordingly.

To investigate the adsorption behaviors of CCPA-P, the pseudo-first and pseudo-second-order adsorption kinetics models were employed – shown in Equations 5 and 6, respectively.

$$\ln\left(\frac{Q_m}{Q_m - Q_t}\right) = k_1 t \tag{5}$$

by plotting $\ln\left(\frac{Q_m}{Q_m - Q_t}\right)$ against time, the gradient of the best fit yields a k_1 value.

$$\frac{t}{Q_t} = \frac{1}{k_2 Q_m^{\ 2}} + \frac{1}{Q_m} t \tag{6}$$

Similarly, by plotting $\frac{t}{Q_t}$ against time, the gradient of the best fit gives both $\frac{t}{Q_t}$ and $\frac{1}{k_2 Q_m^2}$, which are then used to determine k_2 by rearranging the equation. Q_m and Q_t (mg/mg) are the oil adsorption capacities of the aerogel at equilibrium and at the investigated time t (minutes), respectively. The rate constants k_1 and k_2 were determined from the diagrams for pseudo-first and pseudo-second-order models.

3. RESULTS AND DISCUSSION

3.1. Characteristics

Figure 2a presents the synthesized white CCPA material, displaying its ultra-low density. Figure 2b showed the effect of cellulose-to-PVA ratios on the density and porosity of CCPA samples. The densities of the CCPA increased gradually as the cellulose content increased, while the porosities follow an opposite, although not as significant trend. It is certainly expected that the higher cellulose content, the heavier the CCPA samples while simultaneously creating more densely-packed and narrow pores, reducing the volume of the material (Long et al. 2018; Chen et al. 2021). On the other hand, with an increase in cellulose content, the materials would tend to become more fragile due to insufficient PVA content and uneven dispersion of PVA to cross-link with cellulose.

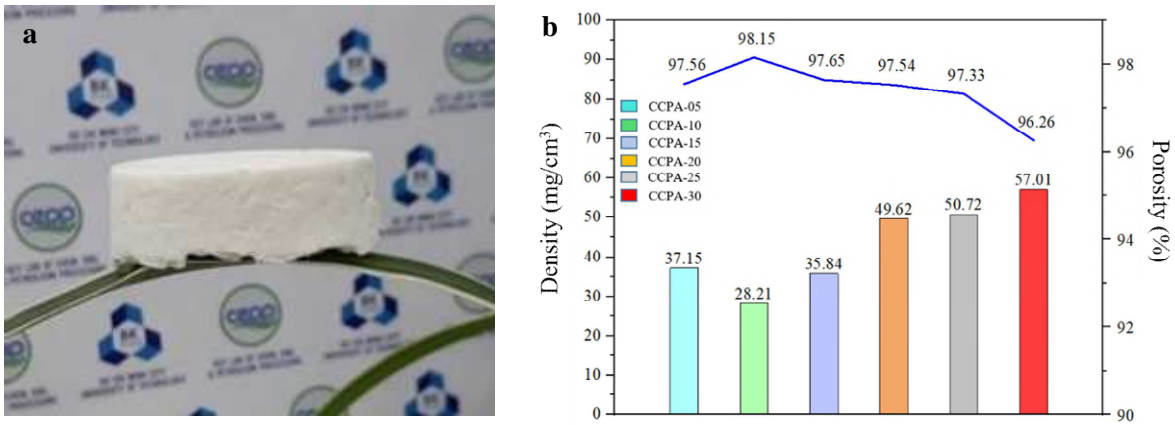

Figure 2. (a) Sample of CPPA, (b) Density and porosity of CPPA

The specific surface areas and average pore sizes were determined via BET adsorption theory. The comparison of specific surface area and average pore size between CCPA-10 with other research is demonstrated in Table 2. As shown, CCPA-10 has a specific surface area and pore size of 80.23 m^2/g and 30.16 nm, respectively. The result additionally showed that CCPA-10 consisted of a mesoporous structure (pore size varying from 2 to 50 nm) (Solano Umaña and Vega Baudrit 2015). These mesopores are well attributed to the formation and sublimation of ice crystals during freeze-drying (Surapolchai and Schiraldi 2010; Khan et al. 2013; Solano Umaña and Vega Baudrit 2015; Long et al. 2018; Chen et al. 2021).

Table 2. Comparison of specific surface area, pore-volume, and average pore size of adsorbent

Materials	Specific surface area (m^2/g)	Average pore size (nm)	References

Cellulose aerogel (Cotton fiber nanocellulose)	13.42	2	(Zhang et al. 2019)
CPPA-10 (coconut peat)	80.23	30.16	This work
Cellulose aerogel (Wood pulp)	153	11.2	(Sehaqui et al. 2011)
Cellulose aerogel (cellulose fiber)	160	14	(Jin et al. 2004)
Cellulose aerogel (rice straw)	178.8	12	(Ferreira et al. 2013)

Figure 3 illustrates microstructure of CCPA through the internal SEM images. CCPA has porous structure on the surface and inner framework (Figure 3a). Especially, as shown in Figure 3b, fiber structure on the surface is generated by the cross-linking of cellulose to have a three-dimensional network. Figure 3c demonstrates the PVA linkage between cellulose particles. The attachment of PVA chain to cellulose can be explain by the forming of hydrogen bond due to both the appearance of hydroxyl groups (–OH) on PVA and cellulose (Figure 3d) (Ghorbel et al. 2019). It can be seen that PVA effectively cross-links with cellulose fibers.

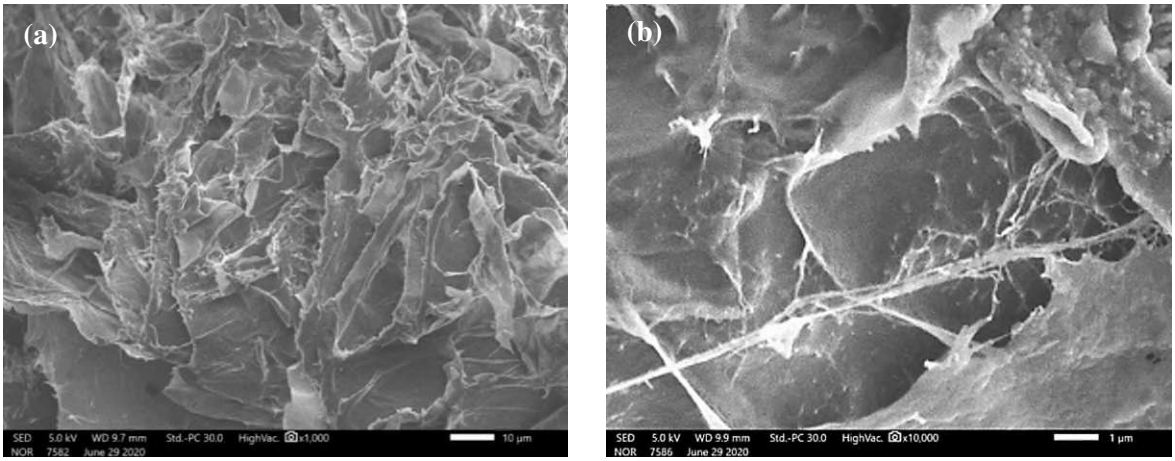

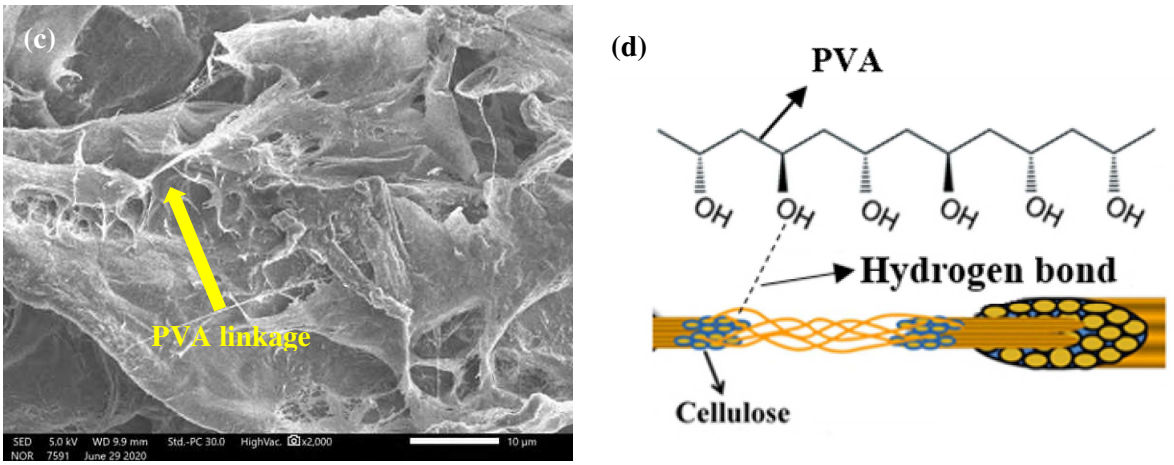

Figure 3. SEM image of (a) porous structure of PPCA, (b) Fiber structure of PPCA, (d) PVA linkage of PPCA, and (d) cross-linking mechanism between cellulose and PVA

The composition of elements in CCPA determined by the EDX spectra is represented in Figure 4. The major elements consisting of carbon and oxygen corresponded to the two oscillating signals with binding energies having the highest intensity. Some common minor elements (Mg, Si, Ca, etc.) are also observed in insignificant amounts (below 1%) for the oscillating tips with lower intensity. The composition of elements in CCPA is categorized into mass ratio and elemental ratio (as shown in Table 3). More specifically, carbon and oxygen accounted for roughly 99.02 % (mass ratio) and 99.61 % (elemental ratio), mostly in form of carbon chains and oxygen-bearing functional groups such as –C=O, –C–O, and –OH in cellulose molecules (Gori et al. 2013). Only 0.98 and 0.49 % of other elements, in terms of mass ratio and elemental ratio respectively, are presented in the synthesized materials. These elements are harmless impurities available in the raw coconut peat.

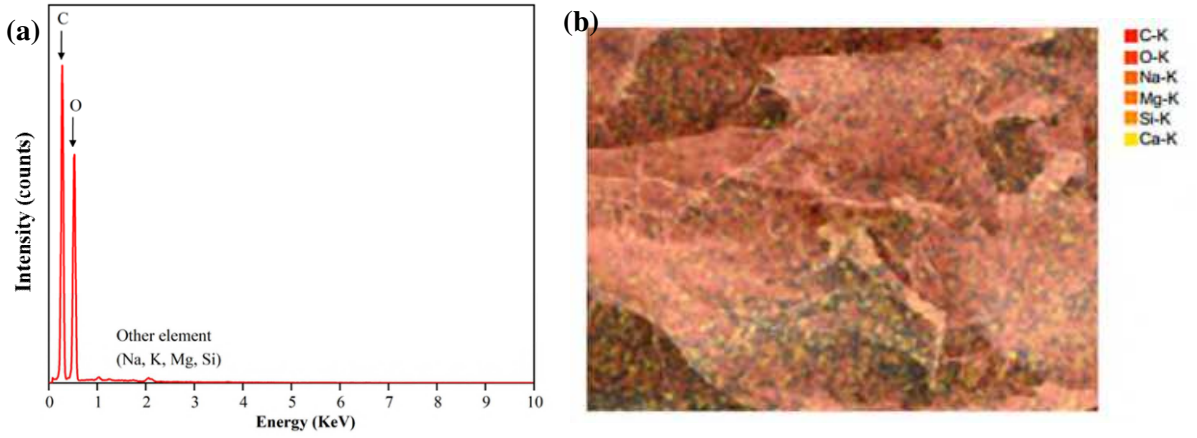

Figure 4. (a) EDX spectrum of CPPA and (b) mapping element of CCPA

Table 3. Mass ratio and element ratio of CCPA

Elements	Mass ratio %	Elemental ratio %
Carbon	48.64±0.09	55.98±0.10
Oxygen	50.38±0.18	43.53±0.16
Other elements (Mg, Si, Ca)	0.98±0.02	0.49±0.01

Figure 5 shows the FTIR spectrum of four distinct samples including coconut peat, cellulose extracted from coconut peat, CCPA, and CCPA-P. The first three samples exhibit two adsorption peaks in the wavenumber region from 3325 to 3600 cm^{-1} and from 2920 to 2960 cm^{-1}, indicating O–H stretching and C–H stretching, respectively (Gori et al. 2013). The characteristic peak of O–H stretching, in particular, is intensified from the spectrum of original coconut peat to that of CCPA due to the exposure of the cellulose content after eliminating lignin and hemicellulose, along with the formation of more hydroxyl groups after the addition of PVA. However, the peak at around 1600-1640 cm^{-1} is assigned to C=O carbonyl stretching of the acetyl groups in hemicellulose or of the α-keto carboxylic acid in lignin, suggesting incomplete treatment (Dilamian and Noroozi 2021). Regarding the CCPA-P spectrum, after being surface-modified with PDMS via dip-coating approach, the emergence of two strong peaks at 1263 and 806 cm^{-1} was observed. The two new peaks are indicative of Si–C vibrational stretching and $-CH_3$ vibrational deformation of siloxane compounds, accordingly (Wan et al. 2015). Meanwhile, the intensity of O–H stretching is significantly weakened due to surface modification with PDMS. It can be explained that each hydrogen atom of the surface –OH groups in cellulose molecules has been replaced by methyl-silane radicals via C–O–Si bonds, creating a hydrophobic surface (Widiyastuti et al. 2019). This confirms the reaction of hydroxyl groups in CCPA with PDMS.

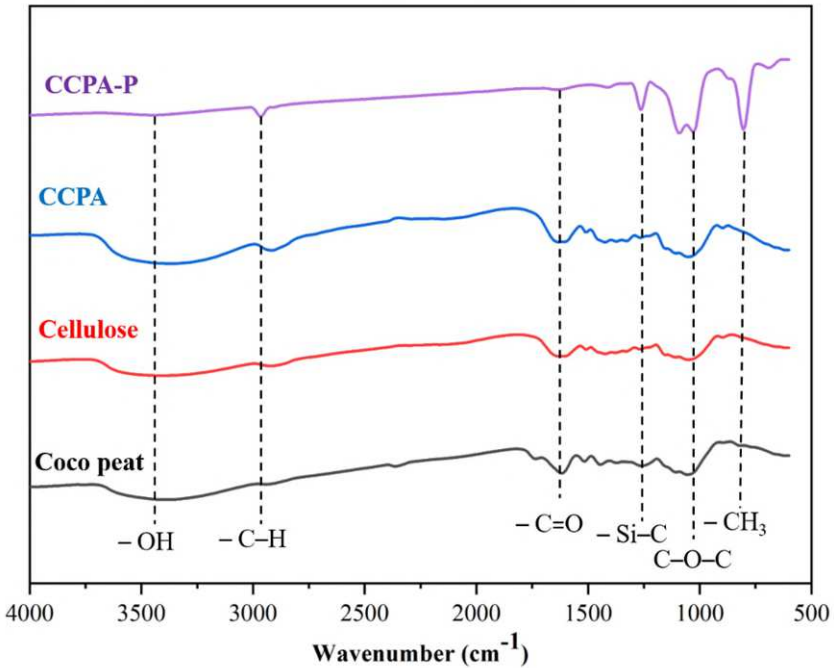

Figure 5. FTIR spectra of coconut peat, cellulose, CCPA, and CCPA-P

Figure 6 illustrates the XRD patterns of cellulose, CCPA, and CCPA-P. The XRD pattern of cellulose possesses characteristic peaks of cellulose type I with partial type II crystal structure, with 2θ values of 16.45°, 22.38°, and 34.39° (Li et al. 2008). Particularly, the characteristic peak at around 16 ° might be the result of the overlapping between $(1\bar{1}0)$ and (110) planes (French 2014; Widiyastuti et al. 2019). The characteristic peak at 2θ = 22.38°, corresponding to the (200) plane, oscillates with the highest intensity, signifying the orderly crystal structure in cellulose (French 2014). However, the XRD pattern

of CCPA exhibits two characteristic peaks at around 20 °, indicating the (110) and (020) planes of cellulose type II crystal structure. Therefore, the obtained material might be partially involved cellulose type II along with cellulose type I crystal structure. This partial conversion of cellulose type II from cellulose type I might be resulted from NaOH treatment. Moreover, XRD pattern of CCPA also possesses a substantial reduction in intensity of the three characteristic peaks which shows that the presence of PVA in CCPA has led to the disorder of the cellulose crystal lattice. And this disorder could lead to the disappearance of the $(1\bar{1}0)$ plane of cellulose type II peak. After being coated with PDMS, the emergence of two characteristic peaks involving a sharp peak at $2\theta = 12$ ° and a broad peak at $2\theta = 22$ ° is observed, corroborating the presence of PDMS on the surface of the CCPA-P (Ferreira et al. 2013). The XRD patterns of all samples are consistent with the results of FTIR studies, verifying a successful PDMS-coating process. Furthermore, the appearance of the peak at $2\theta = 48$ ° in cellulose and CCPA according to the (220) plane of crystalline silicone (Westra et al. 2010; Anuar et al. 2018). This result indicated that the presence of Si in raw coconut peat hasn't been treated completely by NaOH solution (Anuar et al. 2018).

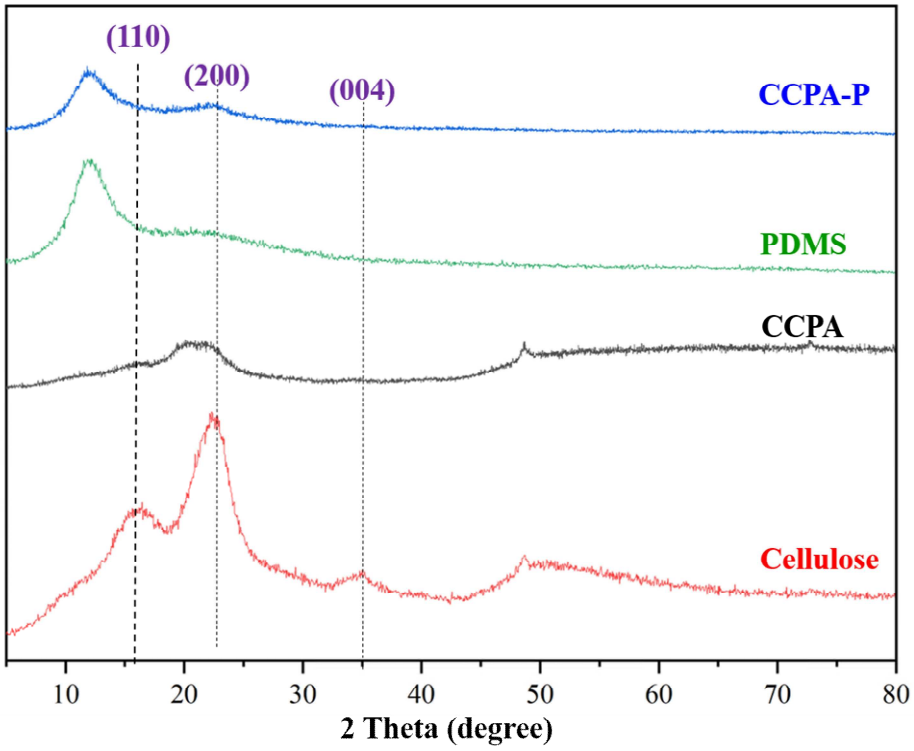

Figure 6. XRD patterns of cellulose, CCPA, PDMS, and CCPA-P

The hydrophobicity of CCPA-P is evaluated through WCA. In Figure 7a, a droplet of water was rapidly spread on the surface of the CCPA and adsorbed onto the material. The hydrophilicity of CCPA can be explained by the appearance of hydroxyl groups on both cellulose and PVA structures forming hydrogen bonds with the water molecules (Wang and Piao 2011). After being modified to obtain CCPA-P, the materials became water-resistant (Figure 7b) by the replacement with methyl-silane radicals via C–O–Si bonds of the hydroxyl groups on PVA and cellulose (Widiyastuti et al. 2019). The

hydrophobicity of CCPA-P is observed by the water contact angle of 114.3° (Figure 7c), implying that CCPA-P is suitable for cleaning up oil spills on the water surface.

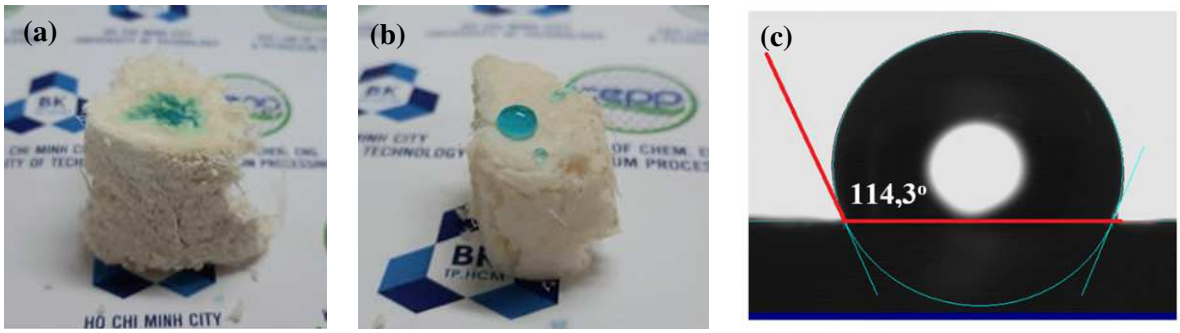

Figure 7. (a) Hydrophilic CCPA, (b) hydrophobic CCPA-P, and (c) water contact angle of CCPA-P

3.2. Oil adsorption

Figure 8a demonstrates the oil adsorption process of CCPA-P for used lubricating oils. First, oil is poured into a water-containing beaker. Then, samples of CCPA-P with different ratios of cellulose to PVA are slowly immersed into the oil layer. The CCPA-P quickly started to adsorb the oil; after 120 seconds, the oil on the water surface is completely adsorbed. The oil adsorption mechanism is elucidated in Fig.8b. After being immersed into the oil/water mixture, the CCPA-P floated on the oil layer surface due to its low density and hydrophobicity. As the oil particles were adsorbed into the porous structure, air is consequently expelled from the porous structure until an equilibrium is reached.

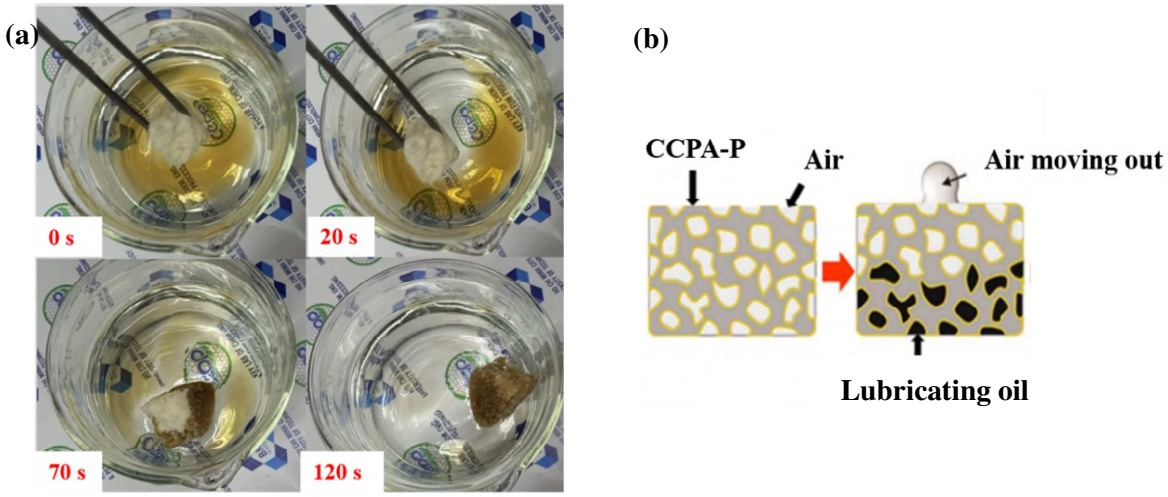

Figure 8. (a) Oil floating on the water surface is completely adsorbed in 120 seconds, (b) Oil adsorption mechanism of CCPA-P

The effect of time on the adsorption process of the various samples of CCPA-P is presented in Figure 9, generally showing the adsorption capacity of all CCPA-P materials reaching equilibrium at the 4-minute mark in both the static adsorption model and the dynamic adsorption model. The results showed that the weight of CCPA-P samples increased 2-3 times after oil was adsorbed at times from 1-10 minutes. The CCPA-P10 sample with cellulose to PVA ratio of 10:1 gives the highest adsorption capacity among the examined samples, with 2.083 and 2.452 mg/mg for static and dynamic models, respectively.

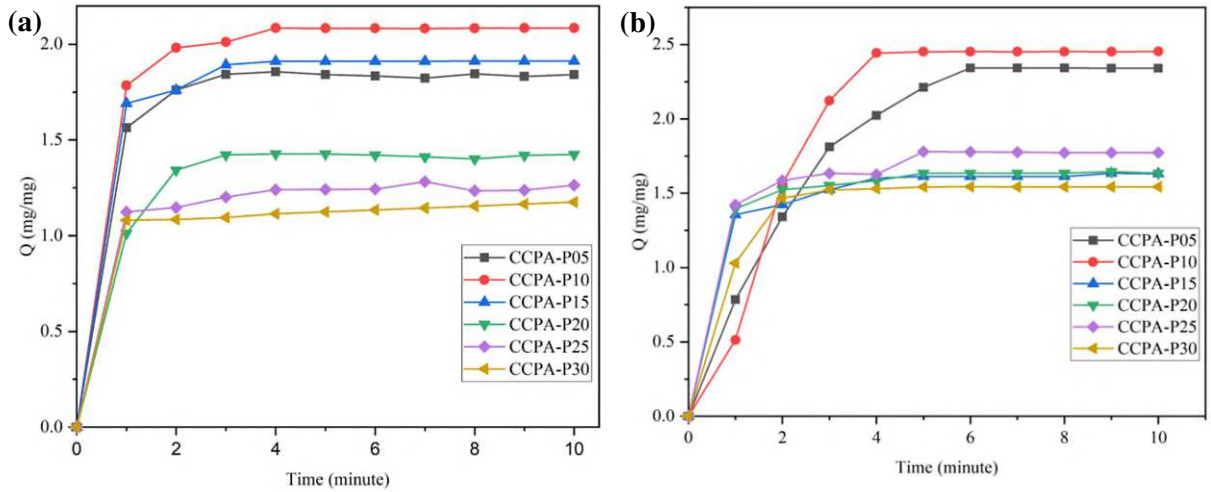

Figure 9. Adsorption capacity over time with (a) static adsorption model and (b) dynamic adsorption model

3.3. Oil adsorption kinetics

Survey results of adsorption kinetics for the six CCPA-P samples according to the static model and the dynamic model are illustrated in Tables 4 and 5. The results showed that the correlation coefficients R^2 of the second-order adsorption model are significantly greater than those of the first-order kinetic adsorption model. This demonstrates that the second-order adsorption kinetic model enables to relatively predict the adsorption function of the CCPA-P materials with oils better than the first-order adsorption model. In addition, the adsorption capacities at the equilibrium point of the dynamic adsorption model are greater than those of the static model since, during mass transfer, the convective diffusion process (corresponding to the dynamic model) will occur rapidly and induce a greater amount of diffusion compared to molecular diffusion (corresponding to the static model) (Grajek et al. 1996).

Table 4. Static adsorption kinetics results

Samples		**CCPA-P05**	**CCPA-P10**	**CCPA-P15**	**CCPA-P20**	**CCPA-P25**	**CCPA-P30**
Q_m (mg/mg)		1.857	2.083	1.911	1.549	1.231	1.123
First-order	R^2	0.984	0.948	0.930	0.915	0.843	0.935
	K_1	1.558	1.341	0.521	0.534	1.881	1.389
Second-order	R^2	0.999	0.995	0.962	0.995	0.988	0.976
	K_2	2.573	0.473	1.316	0.922	5.931	0.887

Table 5. Dynamic adsorption process results

Samples		**CCPA-P05**	**CCPA-P10**	**CCPA-P15**	**CCPA-P20**	**CCPA-P25**	**CCPA-P30**
Q_m (mg/mg)		2.442	2.452	1.613	1.634	1.779	1.542
First-order	R^2	0.983	0.868	0.861	0.854	0.798	0.937
	K_1	0.594	16.89	1.011	0.040	0.282	1.252
	R^2	0.906	0.969	0.998	0.998	0.993	0.993

Second-order	K_2	0.164	0.223	1.384	2.667	1.657	1.427

4. CONCLUSION

In this work, 3D-networked CCPA were synthesized from coconut peat via combining cross-linking with freeze-drying methods. The obtained CCPA were successfully modified into hydrophobic CCPA-P by dip-coating in PDMS and accordingly applied for studying of oil adsorption. The results demonstrated that CCPA-10 with a ratio of cellulose to PVA 10:1 possessed the best properties, with the lowest density of 28.21 mg/cm^3 and the highest porosity of 98.15 %. The maximum adsorption capacity of CCPA-P10 for dynamic models (Q_m = 2.452 mg/mg) is found to be higher than static models (Q_m = 2.083 mg/mg). Studying the adsorption kinetics showed the second-order adsorption kinetic model to more accurately predict the oil adsorption behavior of CCPA-P than the first-order adsorption kinetic model. Therefore, it is reasonable to conclude that CCPA-P10 is promising to become a potential, biodegradable, and eco-friendly oil-absorbing material in the future.

ACKNOWLEDGEMENT

We acknowledge the support of time and facilities from Ho Chi Minh City University of Technology (HCMUT), VNU-HCM for this study.

DECLARATION OF CONFLICTS

We confirm that this work is original and has not been published elsewhere, nor is it currently under consideration for publication elsewhere.

CONFLICTS OF INTEREST

We have no conflicts of interest to disclose. This paper was written by listed authors who are all aware of its content and approve its submission.

ETHICAL STANDARDS STATEMENTS

This study does not involve any human subjects and no animal or human studies were carried out by the authors.

Please address all correspondence concerning this manuscript to corresponding author at nhhieubk@hcmut.edu.vn.

REFERENCES

SAegerter MA, Leventis N, Koebel MM (2011) Aerogels handbook. Springer Science & Business Media

Anuar MF, Fen YW, Zaid MHM, et al (2018) Synthesis and structural properties of coconut husk as potential silica source. Results Phys 11:1–4. https://doi.org/10.1016/j.rinp.2018.08.018

Carmody O, Frost R, Xi Y, Kokot S (2007) Surface characterisation of selected sorbent materials for common hydrocarbon fuels. Surf Sci 601:2066–2076. https://doi.org/10.1016/j.susc.2007.03.004

Chen Y, Wang N, Ola O, et al (2021) Porous ceramics: Light in weight but heavy in energy and environment technologies. Mater Sci Eng R Reports 143:100589. https://doi.org/10.1016/j.mser.2020.100589

268 De Gisi S, Lofrano G, Grassi M, Notarnicola M (2016) Characteristics and adsorption capacities of low-
269 cost sorbents for wastewater treatment: a review. Sustain Mater Technol 9:10–40.
270 https://doi.org/10.1016/j.susmat.2016.06.002
271 Dilamian M, Noroozi B (2021) Rice straw agri-waste for water pollutant adsorption: Relevant
272 mesoporous super hydrophobic cellulose aerogel. Carbohydr Polym 251:117016.
273 https://doi.org/10.1016/j.carbpol.2020.117016
274 Feng J, Wang X, Jiang Y, et al (2016) Study on thermal conductivities of aromatic polyimide aerogels.
275 ACS Appl Mater Interfaces 8:12992–12996. https://doi.org/10.1021/acsami.6b02183
276 Ferreira P, Carvalho Á, Correia TR, et al (2013) Functionalization of polydimethylsiloxane membranes
277 to be used in the production of voice prostheses. Sci Technol Adv Mater 14:55006.
278 https://doi.org/10.1088/1468-6996/14/5/055006
279 French AD (2014) Idealized powder diffraction patterns for cellulose polymorphs. Cellulose 21:885–
280 896. https://doi.org/10.1007/s10570-013-0030-4
281 Ghorbel N, Kallel A, Boufi S (2019) Molecular dynamics of poly (vinyl alcohol)/cellulose nanofibrils
282 nanocomposites highlighted by dielectric relaxation spectroscopy. Compos Part A Appl Sci Manuf
283 124:105465. https://doi.org/10.1016/j.compositesa.2019.05.033
284 Gori Y, Wehrens R, Greule M, et al (2013) Carbon, hydrogen and oxygen stable isotope ratios of whole
285 wood, cellulose and lignin methoxyl groups of Picea abies as climate proxies. Rapid Commun
286 Mass Spectrom 27:265–275. https://doi.org/10.1002/rcm.6446
287 Grajek H, Świątkowski A, Goworek J (1996) The Comparison of the Static and Dynamic Adsorption of
288 Benzene, Methenol and Acetone as Single Adsorbates and Binary Mixtures. In: Fundamentals of
289 Adsorption. Springer, pp 329–336. https://doi.org/10.1007/978-1-4613-1375-5_41
290 Jin H, Nishiyama Y, Wada M, Kuga S (2004) Nanofibrillar cellulose aerogels. Colloids Surfaces A
291 Physicochem Eng Asp 240:63–67. https://doi.org/10.1016/j.colsurfa.2004.03.007
292 Khan I, Elhissi A, Shah M, et al (2013) Liposome-based carrier systems and devices used for pulmonary
293 drug delivery. In: Biomaterials and Medical Tribology. Elsevier, pp 395–443.
294 https://doi.org/10.1533/9780857092205.395
295 Li S, Zhang S, Wang X (2008) Fabrication of superhydrophobic cellulose-based materials through a
296 solution-immersion process. Langmuir 24:5585–5590. https://doi.org/10.1021/la800157t
297 Long L-Y, Weng Y-X, Wang Y-Z (2018) Cellulose aerogels: Synthesis, applications, and prospects.
298 Polymers (Basel) 10:623. https://doi.org/10.3390/polym10060623
299 Rojas-Valencia MN, Galeana-Olvera E, Fernández-Rojas DY, et al (2018) Isolation of cellulose
300 nanofibrils from coconut waste for the production of sewing thread. Adv Mater Sci
301 Sehaqui H, Zhou Q, Berglund LA (2011) High-porosity aerogels of high specific surface area prepared
302 from nanofibrillated cellulose (NFC). Compos Sci Technol 71:1593–1599.
303 https://doi.org/10.1016/j.compscitech.2011.07.003
304 Solano Umaña V, Vega Baudrit J (2015) Micro, meso and macro porous materials on medicine.

http://dx.doi.org/10.4236/jbnb.2015.64023
Surapolchai W, Schiraldi DA (2010) The effects of physical and chemical interactions in the formation of cellulose aerogels. Polym Bull 65:951–960. https://doi.org/10.1007/s00289-010-0306-x
Trevathan JH, Viestenz W (2019) Ecology without sovereignty: Iberian bio-perversity in the work of Manuel Rivas
Udayana SK, Naorem A, Singh NA (2017) The Multipurpose Utilization of Coconut By-Products in Agriculture: Prospects and Concerns. Int J Curr Microbiol Appl Sci 6:1408–1415. https://doi.org/10.20546/ijcmas.2017.606.165
Wan C, Lu Y, Jiao Y, et al (2015) Ultralight and hydrophobic nanofibrillated cellulose aerogels from coconut shell with ultrastrong adsorption properties. J Appl Polym Sci 132. https://doi.org/10.1002/app.42037
Wang C, Piao C (2011) From hydrophilicity to hydrophobicity: A critical review—part II: Hydrophobic conversion. Wood Fiber Sci 43:41–56
Westra JM, Vavruňková V, Šutta P, et al (2010) Formation of thin-film crystalline silicon on glass observed by in-situ XRD. Energy Procedia 2:235–241. https://doi.org/10.1016/j.egypro.2010.07.034
Widiyastuti W, Balgis R, Setyawan H (2019) Production of cellulose aerogels from coir fibers via an alkali–urea method for sorption applications. Cellulose 26:9583–9598. https://doi.org/10.1007/s10570-019-02753-x
Yue X, Zhang T, Yang D, et al (2018) Hybrid aerogels derived from banana peel and waste paper for efficient oil absorption and emulsion separation. J Clean Prod 199:411–419. https://doi.org/10.1016/j.jclepro.2018.07.181
Zhang H, Lyu S, Zhou X, et al (2019) Super light 3D hierarchical nanocellulose aerogel foam with superior oil adsorption. J Colloid Interface Sci 536:245–251. https://doi.org/10.1016/j.jcis.2018.10.038

Figures

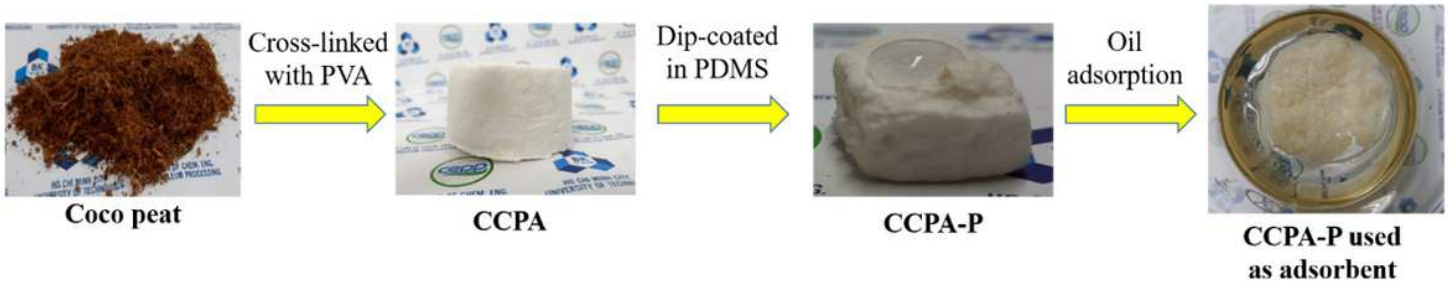

Figure 1

Schematic illustration of the synthesis route and adsorption process of the PPCA-P

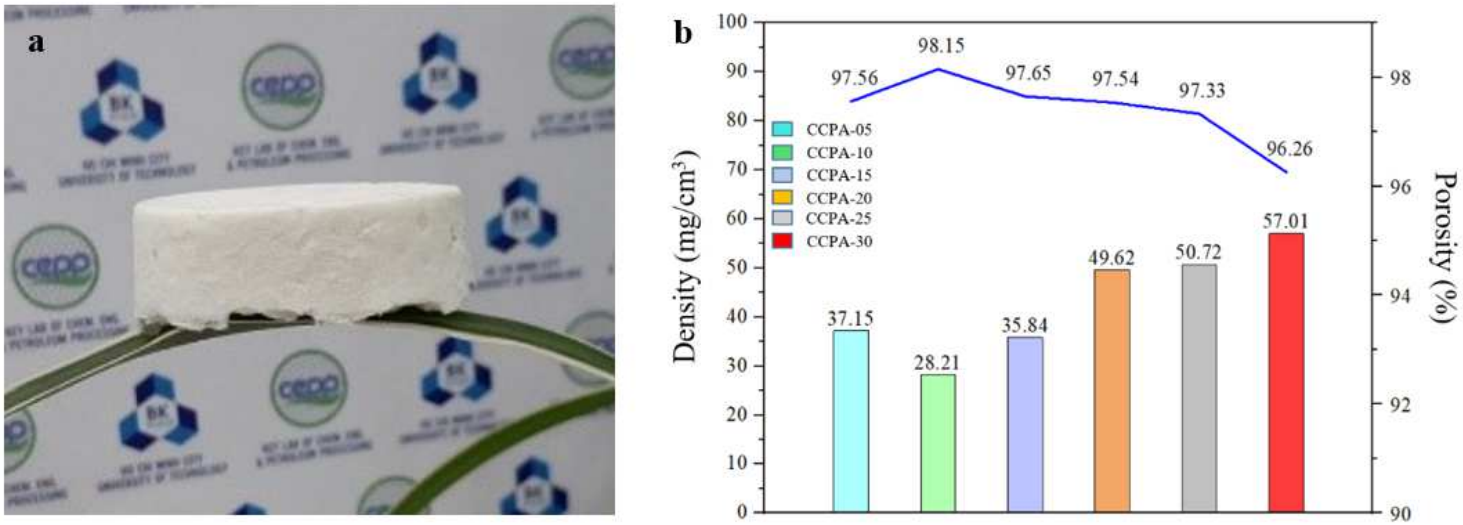

Figure 2

(a) Sample of CPPA, (b) Density and porosity of CPPA

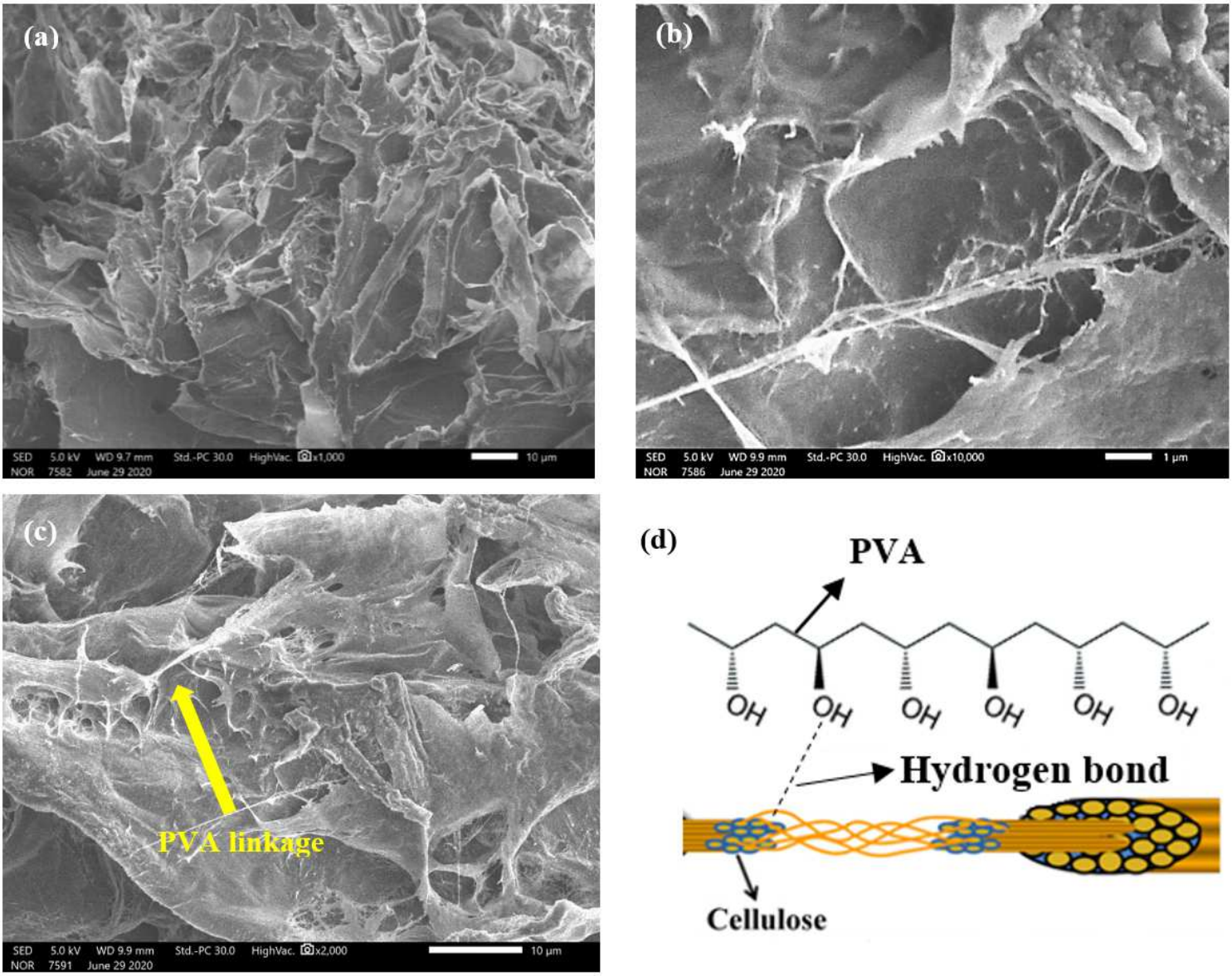

Figure 3

SEM image of (a) porous structure of PPCA, (b) Fiber structure of PPCA, (d) PVA linkage of PPCA, and (d) cross-linking mechanism between cellulose and PVA

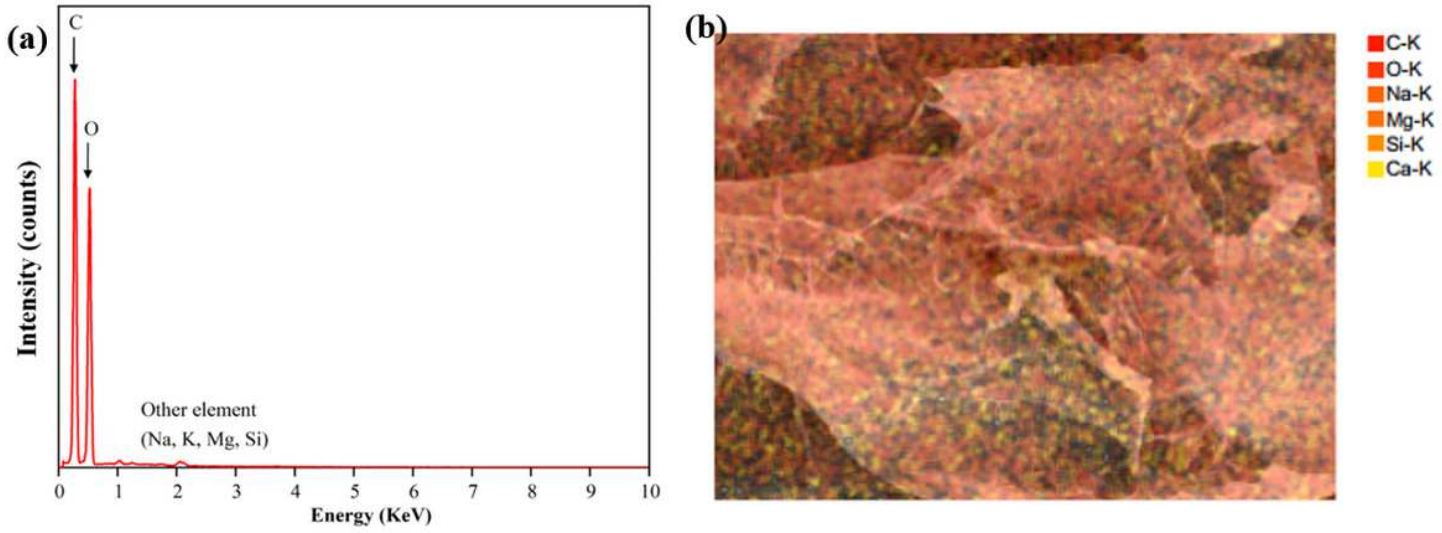

Figure 4

(a) EDX spectrum of CPPA and (b) mapping element of CCPA

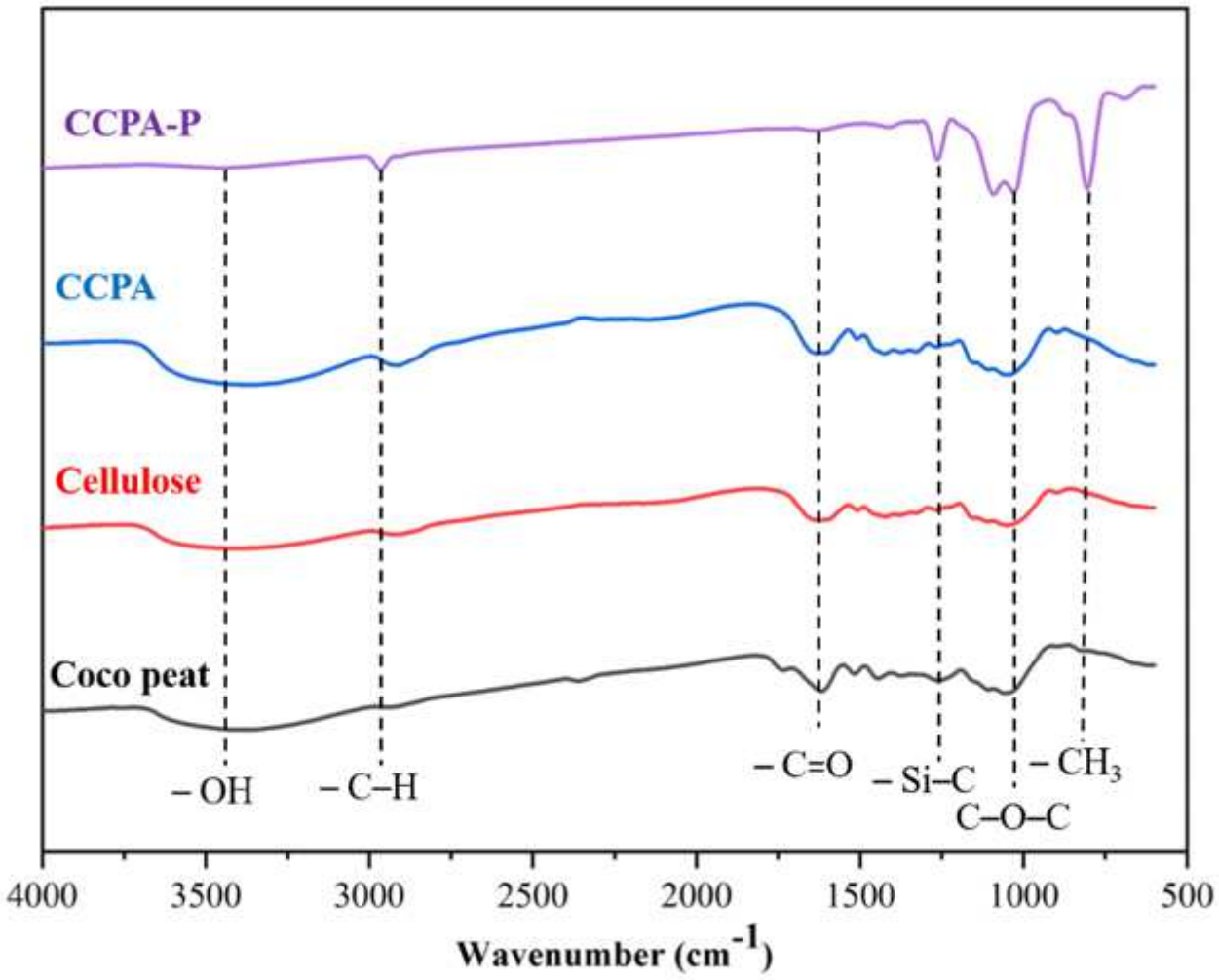

Figure 5

FTIR spectra of coconut peat, cellulose, CCPA, and CCPA-P

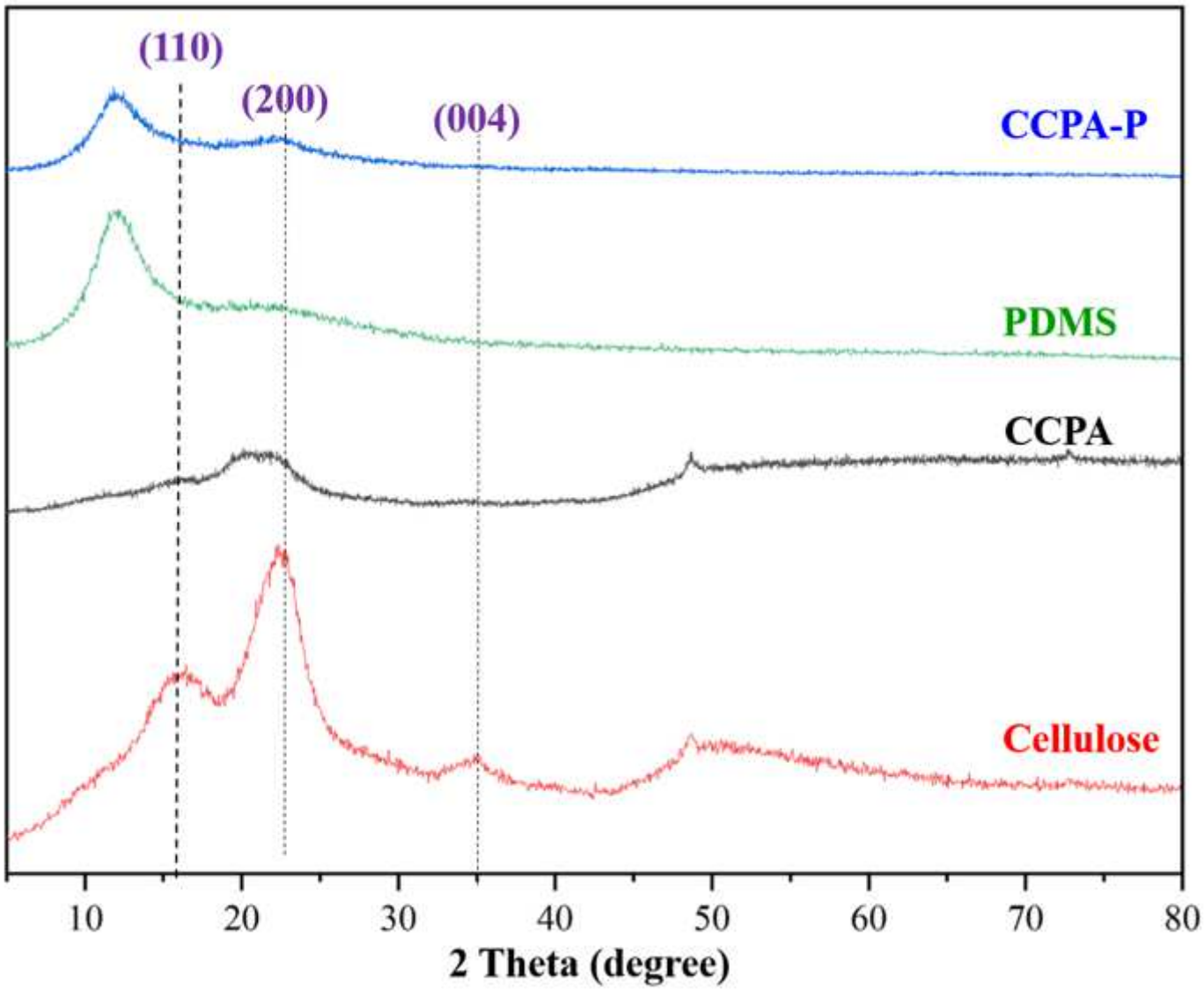

Figure 6

XRD patterns of cellulose, CCPA, PDMS, and CCPA-P

Figure 7

(a) Hydrophilic CCPA, (b) hydrophobic CCPA-P, and (c) water contact angle of CCPA-P

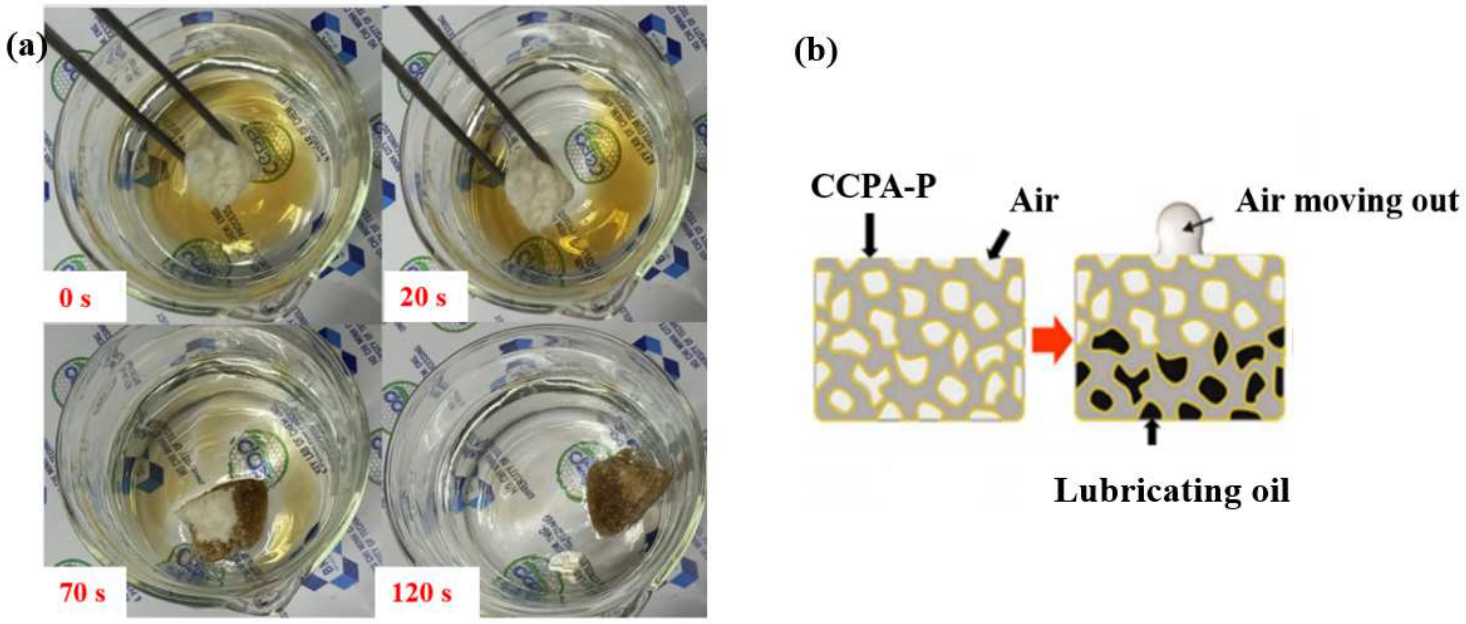

Figure 8

(a) Oil floating on the water surface is completely adsorbed in 120 seconds, (b) Oil adsorption mechanism of CCPA-P

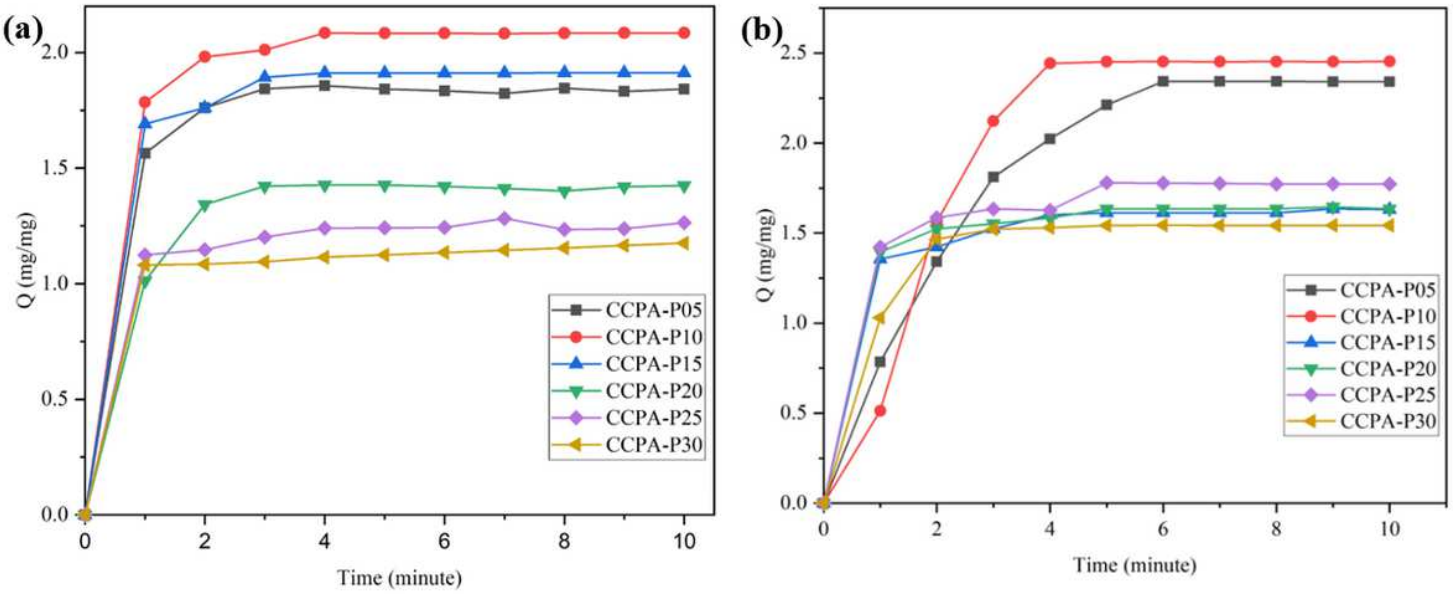

Figure 9

Adsorption capacity over time with (a) static adsorption model and (b) dynamic adsorption model